

# Optimization of hydraulic section of irrigation canals in cold regions based on a practical model for frost heave

Songhe Wang<sup>1a</sup>, Qinze Wang<sup>1b</sup>, Peng An<sup>\*2</sup>, Yugui Yang<sup>3a</sup>, Jilin Qi<sup>4a</sup> and Fengyin Liu<sup>1a</sup>

<sup>1</sup>Institute of Geotechnical Engineering, Xi'an University of Technology, Xi'an, Shaanxi, 710048, China

<sup>2</sup>College of Geology Engineering and Geomatics, Chang'an University, Xi'an, Shaanxi, 710064, China

<sup>3</sup>State Key Laboratory for Geomechanics and Deep Underground Engineering, China University of Mining and Technology, Xuzhou, Jiangsu 221008, China

<sup>4</sup>College of Civil and Transportation Engineering, Beijing University of Civil Engineering and Architecture, Beijing 100044, China

(Received November 25, 2017, Revised January 2, 2019, Accepted January 3, 2018)

**Abstract.** An optimal hydraulic section is critical for irrigated water conservancy in seasonal frozen ground due to a large proportion of water leakage, as investigated by in-situ surveys. This is highly correlated with the frost heave of underlain soils in cold season. This paper firstly derived a practical model for frost heave of clayey soils, with temperature dependent thermal indexes incorporating phase change effect. A model test carried out on clay was used to verify the rationality of the model. A novel approach for optimizing the cross-section of irrigation canals in cold regions was suggested with live updated geometry characterized by three unique geometric constraints including slope of canal, ratio of practical flow section to the optimal and lining thickness. Allowable frost heave deformation and tensile stress in canal lining are utilized as standard in computation iterating with geometry updating while the construction cost per unit length is regarded as the eventual target in optimization. A typical section along the Jinghui irrigation canal was selected to be optimized with the above requirements satisfied. Results prove that the optimized hydraulic section exhibits smaller frost heave deformation, lower tensile stress and lower construction cost.

**Keywords:** frozen soils; seasonal frozen ground; frost heave; irrigation canal; optimal hydraulic section

## 1. Introduction

Irrigation canals, the significant agricultural facilities since ancient times, have been considered as the lifeblood of agriculture that can be hardly replaced (Huang 2014, Zakir *et al.* 2016). Recent surveys prove that an alarming percentage of canals has suffered frost heave induced damage in both canal lining structure and foundation soils, e.g., uplift, swelling and cracks of canal lining, as well as collapse and scouring of foundation soils (Li *et al.* 2015). Two types of frequently encountered damage in irrigation canals in the Loess Plateau are presented in Fig. 1. Except for the collapsible behavior of loess that has drawn particular concerns (Qian *et al.* 2014, Wang *et al.* 2016a, Mei *et al.* 2016, Qian *et al.* 2016), large expenses on maintenance and management for the frost damage due to structure defects and atmospheric circulation are inevitable as the canals were first put into service (Zhu 1991). This results from the conservative method in designing that frost heave induced deformation has not been well included. Hence, the bottleneck in this case is deriving a practical theory for estimating frost heave of irrigation canals.

Both water migration and ice segregation are included in

frost heave of soils (Lai *et al.* 2009). The former necessitates a rational driving force hypothesis, e.g., film water migration, crystallization force, suction force and even the thermomolecular pressure (Dash 1989). Recent works prove that soil freezes with not all water inside transformed into ice and a certain amount of unfrozen water exist even at extremely low temperatures due to the absorptive forces of soil particles (Arenson *et al.* 2005, Romanovsky and Osterkamp 2015). Experimental evidences can be found by nuclear magnetic resonance, differential scanning calorimetry and time domain reflectometry (Liu and Li 2012). The migration of unfrozen water due to the changes in both temperature and salinity can be estimated by the equations proposed by Anderson and Tice (1973) and Kujala (1991).

As for the identification of frozen fringe that is in general required for segregated ice growth, Black and Miller (1990) observed intense phase change in a specific domain and the Darcy's law is satisfied with hydraulic conductivity for many soils decreases with both temperature and unfrozen water content. The thickness of frozen fringe can be measured by X-ray radiography and Charge Coupled Device and is roughly in millimeter range (Akagawa 1988, Watanabe *et al.* 1997). This characteristic thickness also depends on overburden pressure, freezing rate and ice segregating rate (Lai *et al.* 2009). One other point to be concerned is the criterion for ice lens initiation. Black (1995) suggest using pore pressure as the driving force separating soil layers based on the effective stress principle.

\*Corresponding author, Ph.D.

E-mail: [anpeng110@chd.edu.cn](mailto:anpeng110@chd.edu.cn)

<sup>a</sup>Ph.D.

<sup>b</sup>Ph.D. Student



(a) Swelling of lining



(b) Crack of lining

Fig. 1 Frost damage in irrigation canals in loess terrains

Besides, criteria based on the concept of critical separation pressure were proposed (Nixon 1991). Azmatch *et al.* (2012) suggest that the horizontal ice lens formation starts from the cracking of frozen fringe and ice lens initiates close to the ice-entry value on soil freezing curve. Konrad (1993) used the tensile failure strain as the standard to justify whether or not new ice lens is formed.

Considering the significance of frost damage prevention in irrigation canals, a practical method for calculating frost heave of loess was proposed and was then numerically implemented in FLAC. The frequently used arc-bottom trapezoid canal was taken as the study object, and based on three critical geometric indexes such as slope of canal, ratio of practical flow section to the optimal and lining thickness, a novel numerical approach was suggested for optimization of the hydraulic section in loess canal with its geometric feature live updated. Both the frost heave induced deformation and tensile stress in the lining structure were taken as constraints while the construction cost as the target function. Finally, a typical section along the Jinghui irrigation canal was selected to be optimized.

## 2. A practical model for frost heave of clayey soils

### 2.1 Governing equations

Complex ice-water phase change occurred during heat transfer in frozen soils, the multi-phase medium. In practical modeling of engineering behaviors of frozen soils, the following assumptions are generally made for soil itself including incompressibility of soil particles, isotropy and homogeneity of soil, and uniformly distributed pores.

Provided that both convection and radiation are neglected, the heat transfer considering ice-water phase change can be described by Eq. (1) (Yao *et al.* 2012, Wang *et al.* 2014, Yao *et al.* 2016).

$$-h_i + h_v = \rho C \frac{\partial T}{\partial t} \quad (1)$$

with

$$h_i = -\lambda T_i \quad (2)$$

where,  $h_i$  is the heat-flux vector;  $h_v$  is the volumetric heat-source intensity;  $\rho$  is the mass density of the medium;  $C$  is the specific heat at constant volume;  $T$  is the temperature;  $\lambda$  is the thermal conductivity.

A large amount of latent heat due to ice-water phase change will be released or absorbed during freezing or thawing process of the soil. When using the transient heat conduction method, the rapid release or absorption of latent heat will lead to the difficulty in convergence in numerical calculation. In order to solve this problem, the ice-water phase change is assumed to occur within the temperature range of  $[T_b, T_f]$ , with  $T_b$  and  $T_f$  as the lower and upper temperature limits of phase change. Thus, the following two equivalent thermal indexes can be used in modeling including equivalent specific heat  $C^*$  and equivalent heat conductivity  $\lambda^*$ , as shown below in Eqs. (3) and (4).

$$C^* = \begin{cases} C_u & , T > T_f \\ C_f + \frac{C_u - C_f}{T_f - T_b} (T - T_b) + \frac{L}{1 + \theta_w} \frac{\partial \theta_i}{\partial T} & , T_b \leq T \leq T_f \\ C_f & , T \leq T_b \end{cases} \quad (3)$$

$$\lambda^* = \begin{cases} \lambda_u & , T > T_f \\ \lambda_f + \frac{\lambda_u - \lambda_f}{T_f - T_b} (T - T_b) & , T_b \leq T \leq T_f \\ \lambda_f & , T \leq T_b \end{cases} \quad (4)$$

where, the subscripts  $u$  and  $f$  denote soils in unfrozen and frozen states;  $L$  is the latent heat due to ice-water phase change;  $\theta_w$  and  $\theta_i$  are the volumetric contents of water and ice. This method has been successfully applied in engineering design for various lifeline projects in Qinghai-Tibetan plateau such as bridges, highways and irrigation canals (Lai *et al.* 2005, Qi *et al.* 2007, Li *et al.* 2015).

Despite heat transfer, migration of water is the other key issue during soil freezing. For simplicity, vapor flow and ice phase movement are neglected here. Based on the point by Black (1999) that water movement in frozen fringe can be simplified as the Darcy's flow, Eq. (5) proposed by Li *et al.* (2015) can be utilized to describe the water migration in the whole domain.

$$\frac{\partial \theta_w}{\partial t} = \text{div} [k^* \text{grad}(\psi)] \quad (5)$$

where,  $k^*$  is the hydraulic conductivity of soils;  $\psi$  is soil water potential, generally taken as the driving force of water migration, as shown in Eq. (6).

$$\psi = P_w + G \quad (6)$$

where,  $P_w$  is the pore water pressure;  $G$  is the gravity potential. In most cases, the gravity potential of fluid flow is limited within freezing soils and can be neglected here. Thus, the pore water pressure is regarded as the primary force inducing water flow in freezing soils. A general form of the Clapeyron equation is introduced here to model the correlations of ice pressure and water pressure versus soil temperature (Ma *et al.* 2015), as given below in Eq. (7).

$$\frac{P_w}{\rho_w} - \frac{P_i}{\rho_i} = L \ln \left( \frac{T_k}{T_0} \right) \quad (7)$$

where,  $P_i$  is the ice pressure and is taken to be zero for sake of simplicity;  $\rho_i$  and  $\rho_w$  are the densities of ice and liquid water, respectively;  $T_k$  is the absolute temperature;  $T_0$  is the temperature for ice-water phase change at a standard atmospheric pressure.

Following the work by Lai *et al.* (2009), the volumetric water content  $\theta_w$  considering both the contributions of unfrozen water and ice can be described by the following Eq. (8).

$$\theta_w = \theta_u + \frac{\rho_i}{\rho_w} \theta_i \quad (8)$$

where,  $\rho_w$  and  $\rho_i$  are the densities of water and ice, respectively.

Considering the fact that soil freezes with not all water inside transformed into ice and a certain amount of unfrozen water exist even at extremely low temperatures (Arenson *et al.* 2005, Romanovsky and Osterkamp 2015), the unfrozen water content can be empirically determined by the Eq. (9) as shown below.

$$\theta_u = a |T|^{-b} \quad (9)$$

where  $a$  and  $b$  are experimental parameters.

Based on the work by Wang *et al.* (2016b), the hydraulic conductivity for soils in thawed state, frozen state and frozen fringe can be empirically determined by Eq. (10).

$$K(T) = K(T_{ref}) \frac{\mu(T_{ref})}{\mu(T)} \quad (10)$$

where,  $\mu(T)$  is the viscosity of water at temperature  $T$ ;  $T_{ref}$  is the reference temperature, equal to 20°C, the ambient temperature in laboratory.

The conservation equation for fluid flow can be given in the following form.

$$-q_{i;i} + q_v = \frac{1}{M} \frac{\partial p}{\partial t} + \alpha \frac{\partial \varepsilon_v}{\partial t}, \quad \varepsilon_v = \varepsilon_{ii} \quad (i=1,2,3) \quad (11)$$

where,  $q_v$  is the volumetric fluid source intensity;  $\alpha$  and  $M$  are the Biot's coefficient and modulus, respectively. Provided that soil particles are negligible,  $\alpha=1.0$  and  $M=k_w/\eta_0$ , with  $k_w$  as the volumetric modulus of water and  $\eta_0$  the void ratio of soils.

The stress-strain relationship for frozen soils can be described as (Lai *et al.* 2005, Li *et al.* 2016).

$$\{\Delta \sigma\} = [D_T] \{\Delta \varepsilon_e\} \quad (12)$$

with  $\{\Delta \varepsilon_e\}$  as the elastic strain increment, and its specific form is shown below in Eq. (13).

$$\{\Delta \varepsilon_e\} = \{\Delta \varepsilon\} - \{\Delta \varepsilon_v\} - \{\Delta \varepsilon_p\} \quad (13)$$

where  $\{\Delta \varepsilon\}$  denotes the strain increment;  $\{\Delta \varepsilon_v\}$  is the frost heave strain increment; and  $\{\Delta \varepsilon_p\}$  represents the plastic strain increment.

Frost heave characterizes the volumetric deformation of soils during freezing, resulted from both a phase transition from liquid water to ice and pore water freezing in-situ. Ascertaining the location of ice segregated in freezing front and its thickness is not taken into account for sake of simplicity. Three main components of deformation are considered in computing the frost heave deformation of soils, i.e., the volume expansion due to the frozen of migrated water, the volume change due to the variation of unfrozen water and soil pores (Lai *et al.* 2005). The frost heave strain of soils is given in Eq. (14) (Lai *et al.* 2005).

$$\varepsilon_v = 1.09(\theta_0 + \Delta \theta_w - \theta_u) + \theta_u - n_0 \quad (14)$$

where,  $\theta_0$  is the initial water content;  $\Delta \theta_w$  is the increment of migrating water.

Because both frozen and unfrozen soils are both considered to be isotropic, and the expansion strain in each direction is equal (Lai *et al.* 2005). Hence, the  $\{\varepsilon_v\}$  at plane strain condition could be expressed in Eq. (15).

$$\{\varepsilon_v\} = \frac{1}{3} \varepsilon_v \{1 + \nu_T \quad 1 + \nu_T \quad 0\}^T \quad (15)$$

Following the work by Wang *et al.* (2016b), compression of soils in both thawed and 'cold' frozen domain can be calculated based on a Drucker-Prager yield criterion, as shown below in Eq. (16).

$$\alpha I_1 + \sqrt{J_2} = k_1 \quad (16)$$

with

$$\alpha_1 = \frac{2 \sin \phi}{\sqrt{3}(3 - \sin \phi)}$$

$$k_1 = \frac{6c \cos \phi}{\sqrt{3}(3 - \sin \phi)}$$

where, the parameters  $c$  and  $\phi$  are the cohesion and angle of internal friction. Note that the 'warm' and 'cold' frozen soils were classified based on a temperature limit proposed by Qi and Zhang (2008), i.e., -1.0°C.

Experiments have proven that the mechanical properties of frozen soils show close correlations with temperature (Li *et al.* 2015) and can be estimated by Eq. (17).

$$M_i = a_i + b_i |T|^{m_a} \quad (17)$$

where,  $M_i$  ( $i=1-4$ ) are mechanical parameters of frozen soils, with 1-4 represent elastic modulus, Poisson's ratio, cohesion and internal friction angle, respectively; Experimental parameters  $a_i$  and  $b_i$  can be fitted from test results, with the first denoting the mechanical parameter of soils in thawed state. For thawed soils, the parameters of  $b_i$  ( $i=1-4$ ) are equal to zero. The parameter  $m_a$  can be taken to

be 0.6 for the elastic modulus of frozen clayey soils (Lai *et al.* 2009) while for the other three parameters,  $m_a$  is equal to 1.0.

## 2.2 Experimental verification

### (1) Geometric model and parameters

A typical section along the Beiying Canal located in Heilongjiang Province, China, is taken as an example (Li *et al.* 2015). Based on the similarity theory (Lai *et al.* 2009), the relationship of similarity ratio is given below in Eq. (18).

$$C_T \cdot C_t = C_l^2 \quad (18)$$

where  $C_T$ ,  $C_t$ ,  $C_l$  are dimensionless temperature, time and geometry ratios of the prototype to the model, respectively. For this model test,  $C_T=1.5$ ,  $C_t=16.7$ ,  $C_l=5$ .

The liquid and plastic limits for the clay used are 50.9% and 26.4%, respectively. The dry density was controlled to be 1.55 g/cm<sup>3</sup> while the canal model was watered for 20 days. The geometric model used in modeling is identical to the model produced, as presented in Fig. 2. The upper boundary was adjusted by a controlled environmental temperature (Fig. 3) while the bottom maintained at 3.0-4.0°C. The physical and mechanical parameters used in numerical modeling are listed in Tables 1 and 2, respectively.

### (2) Comparison of calculated and measured data

Fig. 4(a) presents the comparisons of calculated and measured temperatures at three points, i.e., T2-0.2, T4-0.2, and T6-0.2, with T2, T4 and T6 denoting the three temperature monitoring points in Fig. 2 and ‘0.2’ representing the depth of the selected points. The points at the depth of not larger than 0.2 m are taken to illustrate the development of thermal regime in that soils in shallow layers have exhibited a sharp decrease in temperature with the environment, as shown in Fig. 3. Besides, the calculated temperatures at the three points all agree well with the original data, as can be easily noted from the figure that the data points are all close to the straight line of  $y=x$ . The mean absolute percentage errors (MAPEs) for the three selected points are 3.37%, 5.39% and 6.90%, respectively. Comparison of measured and calculated displacements in vertical and horizontal positions is plotted in Fig. 4(b). Here, only the monitored displacements in the position of S2 are used in the comparison due to the availability of test data presented in the literature (Li *et al.* 2015). It can be easily noticed that the calculated displacement based on the Drucker-Prager yield criterion shows good agreement with the monitored data. Most of the data points lie around the straight line of  $y=x$ , with a relatively small deviation between the calculated and measured data. The MAPEs for the vertical and horizontal positions are 8.33% and 5.41%, respectively. It proves the rationality of the calculated temperatures and displacements of the model.

Considering the fact that only the monitored data at a duration of 198 h was given in the literature (Li, *et al.* 2015), the vertical displacements of the three monitoring points S1, S2 and S3, corresponding to the toe, slope surface and shoulder of the model, are presented in Fig. 5.

Table 1 Physical parameters for clay in Beiying Canal (data from Li *et al.* 2015)

Physical index	Data
Specific heat, $C$ , kJ/(kg·°C)	
in frozen state	1.15
in thawed state	1.51
Heat conductivity, $\lambda$ , W/(m·°C)	
in frozen state	2.00
in thawed state	1.33
Permeability, $K(T_{ref})$ , 10 <sup>-5</sup> m/s	1.50
Unfrozen water content, $\theta_u$ , %	
$a$ , %/°C	0.34
$b$	0.17

Table 2 Mechanical indexes for clay in Beiying Canal (data from Li *et al.* 2015)

Parameters	Data
$a_1$ , MPa	22.5
$b_1$ , MPa/°C	11.3
$a_2$	0.28
$b_2$	-0.007
$a_3$ , kPa	20.0
$b_3$ , kPa/°C	11.7
$a_4$ , °	20.0
$b_4$ , °/°C	0.59

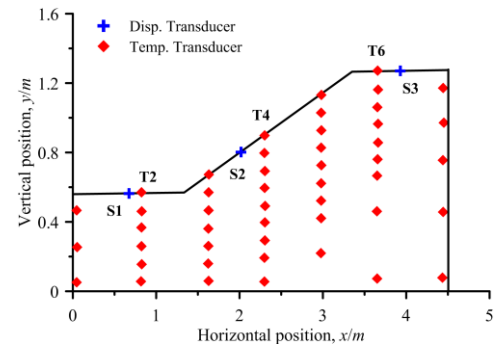


Fig. 2 Geometric model for Beiying Canal

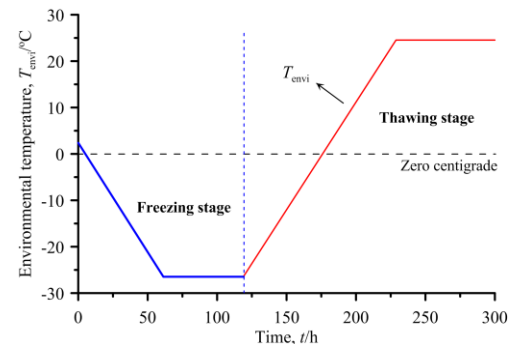


Fig. 3 Environmental temperature during testing

The calculated results by the practical method in this study as well as that based on the method by Li *et al.*

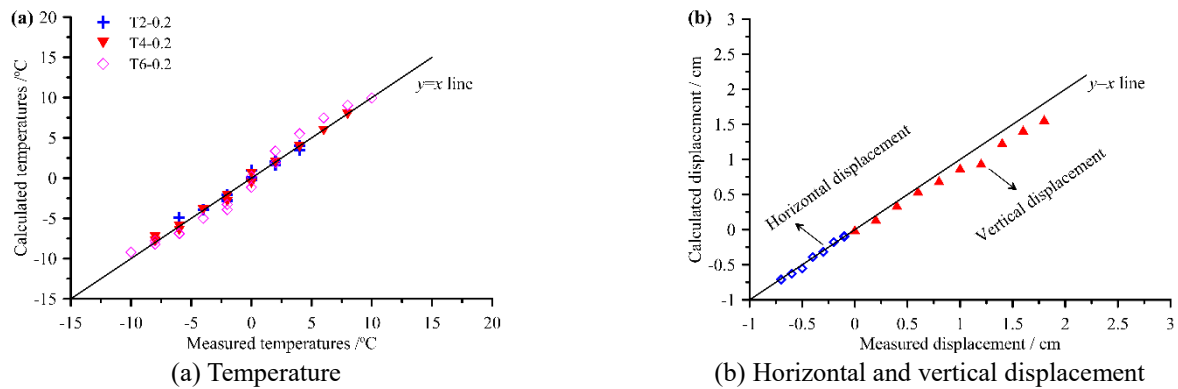


Fig. 4 Comparison of calculated and measured data

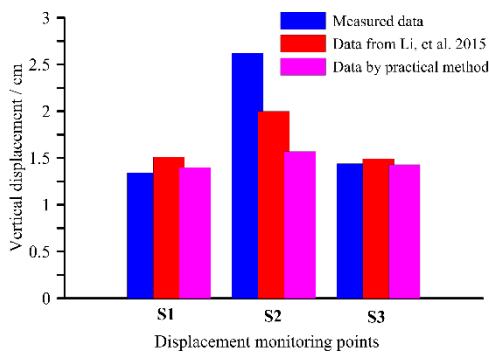


Fig. 5 Comparison of calculated and measured displacements

(2015) are also plotted as the purple and red rectangles in Fig. 5, respectively. Clearly it proves that the calculated displacements by the proposed practical method agree in general with the test data. The MAPEs for the calculated data based on the two methods are 13.27% and 15.08%, which indicates that the practical method exhibits a slightly higher deviation than that by Li *et al.* (2015). However, a better agreement can be noted for the points S1 and S3, i.e., the toe and shoulder of the model, while for the point S2, the maximum vertical displacement calculated by the method proposed in this study is about 1.57 cm, which is slightly lower than the monitored data.

Compared to the viscoplastic constitutive relationship proposed by Li, *et al.* (2015), the practical method has not considered the effect of viscous behavior of soils, i.e., the time-dependent effect. This kind of treatment will be of great help in improving the calculation efficiency to a large extent, and is also simpler in deriving equations when carrying out the frost heave deformation computation. The other factor worthy of attention is that the viscous deformation or creep will become an important factor that must be considered in long-term settlement calculations (Wang, *et al.* 2016). But for frost heave of soils in seasonal frozen ground, this physico-mechanical process, which occurs in the freezing period, has a relatively small contribution to the total deformation. This deformation should be taken into account only when ‘warm’ frozen soils are involved (Wang, *et al.* 2014). The deviation at the second characteristic point may be attributed to two main aspects: experimental error and the rationality of numerical parameters. For the first one, the uniformity of the model

produced in the horizontal and vertical directions, the monitoring error of the instrument, etc. may lead to this particular error. Moreover, the calculation parameters derived from test results of a relatively uniform soil may also account for this kind of deviation.

### 3. Optimization of hydraulic section: numerical approach

#### 3.1 Key technical problems in computation

A live development of thermal regime results in a considerable change in engineering behaviors such as water migration, heat transfer and mechanical responses. Besides, the determination of the optimal hydraulic section still relies on the hydraulic regime as revealed by experiences of engineers while little work has focused on the negative effect of frost heave. Thus, the computational method should also be updated, especially the synchronization of hydro-thermal computation. Three main problems encountered when carrying out numerical modeling as shown below.

(1) Live computation of frost heave and compression in corresponding domains

Frost heave of canal foundation originates from the phase change of both migrated and in-situ water into ice, and for soils at higher water contents, the volumetric expansion primarily results from the migrated water under dual effect of gradient of both temperature and soil water potential in essence. Thus, a rational thermal regime calculated at a minus-temperature boundary will facilitate the determination of ice-water phase change domain in the whole computational area and then the frost heave strain can be obtained based on the equation by Lai *et al.* (2005). Note that the temperatures for the two types of ice-water phase change, i.e., thawing and freezing, never coincide due to the principle of entropy increase and the hysteresis behaviors can be noticed from the correlations of volumetric water content versus temperatures (Lu *et al.* 2017). Thus, for sake of simplicity a characteristic index obtained from the equilibrium freezing stage of the freezing curve is utilized, i.e., the freezing point.

In previous numerical work for cold regions engineering, the thermal, hydraulic and mechanical

computations were all accomplished in identical domains; however, the problem mentioned above necessitates a live calculation of frost heave and compression in their corresponding domains, with thermal computation within the whole. With development of thermal regime, the affected areas for frost heave and compression both vary and require a live determination. Here a section of codes compiled by Fish language are embedded into the main program and easily solved this tough problem. Based on the thermal regime calculated for one time step, a section of code for identifying whether or not soils are frozen is iterated through each element in the whole domain. The computational modes for fluid flow and mechanical response will be turned on if a negative result is reached, i.e., *set ther off fluid on mech on*, which is a section of code that is written in Fish language and can be executed by the main program of FLAC. Otherwise, only the mechanical mode is initiated within the ‘cold’ frozen domain, i.e., *set ther off fluid off mech on*, while in ‘warm’ frozen area, computational modes like the first are activated, i.e., *set ther off fluid on mech on*. Note that the ‘warm’ frozen domain represents the domain with element temperatures ranging from zero to  $-1.0$  °C.

(2) Synchronization of hydraulic and thermal computations

Thermal and hydraulic computations are controlled by their particular timesteps respectively, i.e., *thdt* and *gwdt* and the runtime also differs. This required a synchronization of the two computational modes (Itasca 1999). Each timestep for both hydraulic and thermal computations should not exceed the critical value  $dt_{cr}$  in explicit algorithm to ensure numerical stability, i.e., Eq. (19) should be satisfied.

$$\begin{cases} gwdt_{cr} \leq \frac{L_c^2}{c_{gw}} \\ thdt_{cr} \leq \frac{L_c^2}{c_{th}} \end{cases} \quad (19)$$

where,  $gwdt_{cr}$  and  $thdt_{cr}$  are the critical timesteps for hydraulic and thermal computations, respectively;  $L_c$  is the minimal size of grid cells;  $c_{gw}$  and  $c_{th}$  are the diffusivities for fluid and heat, respectively.

For cases introduced here,  $gwdt_{cr} < thdt_{cr}$  and thus,  $thdt_{cr} = N \times gwdt_{cr}$ , with  $N$  as an integer, implying that one cycle of coupled computation includes one timestep for thermal mode and  $N$  timesteps for hydraulic mode. If  $T_{ij} \geq 0$  °C, then as both thermal and hydraulic modes synchronized, the timesteps for hydraulic and mechanical modes should also be adjusted to ensure the rigid body equilibrium, i.e.,  $n_{gw} = N_1 \times n_{mech}$ , with  $N_1$  as an integer while both thermal and mechanical modes should be synchronized if  $T_{ij} \leq 0$  °C. The criterion shown in Eq. (20) should be satisfied in this case.

$$\frac{\Delta t_{ther}}{\Delta t_{mech}} = \sqrt{\frac{\rho}{K + (4/3)G}} \frac{L_c}{c_{th}} \quad (20)$$

where,  $\Delta t_{ther}$  and  $\Delta t_{mech}$  are timesteps for thermal and mechanical modes, respectively;  $\rho$  is density of materials;  $K$  is the volumetric modulus;  $G$  is shear modulus. The above

timesteps and integers  $N$  and  $N_1$  are determined by trial.

(3) Optimization of hydraulic section considering both geometry and frost heave

The trapezoid canal with arc-bottom is one of the frequently used section forms in Northern China, and is characterized by flow stability, small amplitude of flow depth and good resistance to sediment deposition and washout. Fig. 6 illustrates a typical section of the trapezoid canal with arc-bottom. Besides, the merit to be particularly concerned is the anti-frost performance. Three standards should be satisfied when running an irrigated canal in seasonal frozen ground, i.e., i) good discharge capacity with the cross section close to the optimal hydraulic section, ii) no cracks formed in canal lining, and iii) never exceed an allowed frost heave deformation. Meanwhile, the land conservation, lower cost and convenience in construction should also be taken into account when constructing.

The depth of water for the optimal hydraulic section for the trapezoid section with arc-bottom can be calculated based on the Technical code for seepage control engineering on canal (GB/T50600—2010, 2011), with a general form shown in Eq. (21).

$$h_0 = 1.542 \left[ \frac{nQ}{(2m + \theta)\sqrt{i}} \right]^{3/8} \quad (21)$$

where,  $Q$  is the designed flow of the canal;  $i$  is the longitudinal slope of the canal;  $n$  is the coefficient of roughness for the canal lining. From the above equation, the depth of  $h_0$  can be determined by a set of parameters, i.e.,  $Q$ ,  $i$ ,  $n$  and  $m$ . If the parameters  $Q$ ,  $i$  and  $n$  are given, the depth of  $h_0$  can be uniquely identified by specifying the value of the parameter  $m$ .

However, the optimal hydraulic section cannot be fully satisfied in various site conditions so that both the opening width and depth of the cross section have to be adjusted to meet a more economic need. Thus, the practical economic section by appropriately changing the geometric character of the cross-section is mostly used in practical engineering. Two basic requirements should be satisfied for this practical section, i.e., 1) the designed flow should be identical to that in the optimal condition; and 2) adapt to local site conditions with investment saved. From the technical code, a unique relationship can be satisfied between the optimal hydraulic section and the practically economic section, as shown below in Eq. (22).

$$AK_r^2 + BK_r + C = 0 \quad (22)$$

with

$$A = (2m - 2\sqrt{1+m^2} + \theta)^2 - 2\alpha^4(2m + \theta)(0.5\theta + 2m - 2\sqrt{1+m^2})$$

$$B = 4\sqrt{1+m^2}(2m - 2\sqrt{1+m^2} + \theta) - 4\alpha^4(2m + \theta)(\sqrt{1+m^2} - m)$$

$$C = 4(1+m^2) - 2\alpha^4(2m + \theta)m$$

where,  $K_r$  denotes the ratio of the radius of arc-bottom to the depth of water for the practical economic section;  $\alpha$  is the ratio of practical economic section to the optimal hydraulic section.

Solve the above equation, we can get a practical solution in Eq. (23).

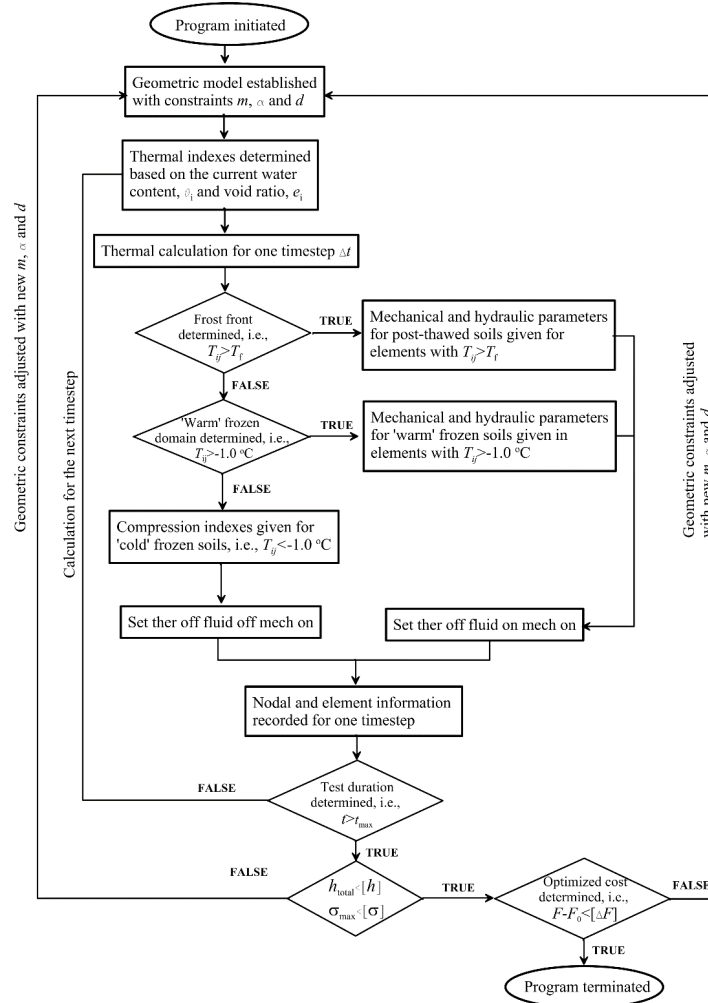


Fig. 7 Computational procedure for hydraulic section optimizing

$$K_r = \frac{-B + \sqrt{B^2 - 4AC}}{2A} \quad (23)$$

From the above equation, the parameter  $K_r$  can be considered as a function of both  $m$  and  $a$ . The normal depth of flow in the practical economic section,  $h_1$ , can be obtained by Eqs. (24) and (25).

$$h_1 = \frac{(2m + \theta)\alpha^{2.5}}{(2m - 2\sqrt{1+m^2} + \theta)K_r + 2\sqrt{1+m^2}} 1.542 \left[ \frac{nQ}{(2m + \theta)\sqrt{i}} \right]^{3/8} \quad (24)$$

$$r / h_1 = K_r \quad (25)$$

Clearly it shows that a set of data  $m$  and  $a$  can uniquely determine a normal depth of flow for the arc-bottom trapezoid canal at given parameters of  $Q$ ,  $i$  and  $n$ . Thus, two independent parameters can be noted in determining the exterior geometric feature of canals, i.e.,  $m$  and  $a$ . The variables in designing a arc-bottom trapezoid canal can be generalized into a simple function of  $X(m, a, d)$  for simplicity, with  $d$  as the thickness of canal lining that may induce larger variance in tensile stresses in canal lining structure. Little change can be noted in the discharge cross section as the ratio of radius of arc to the flow depth

changed. The practically economic section with an area growth not exceeding 3%-4% of the optimal is utilized, i.e.,  $1.0 \leq \alpha \leq 1.04$ . Take the ratio of practical flow section to the optimal as a geometric constraint while both the allowed tensile stress in canal lining and frost heave induced deformation as performance constraints. The mathematical equations for optimizing the hydraulic section of arc-bottom trapezoid canals in seasonal frozen ground are given below.

$$\begin{aligned} \min F &= B_1 \times F_1 + A_q \times F_2 + 1 \times A_c \times F_3 \\ A_c &= 2d[(h_1 + h_2)\sqrt{1+m^2} - h_1 K_r (\sqrt{1+m^2} + m)] + d\pi K_r h_1 \text{arc cot } m / 45^\circ \\ A_q &= K_r^2 h_1^2 (\text{arc cot } m + 2m - 2\sqrt{1+m^2}) + 2K_r h_1 (h_1 + h_2)(\sqrt{1+m^2} - m) + m(h_1 + h_2)^2 \end{aligned}$$

S.t

$$\begin{aligned} m_{\min} &\leq m \leq m_{\max} \\ d_{\min} &\leq d \leq d_{\max} \\ 1.0 &\leq \alpha \leq 1.04 \\ h_{\max} &\leq [h_\sigma] \\ \sigma_{\max} &\leq [\sigma] \end{aligned}$$

where,  $d_1$  is the width of jointing;  $h_2$  is the freeboard of the canal;  $h_{\max}$  is the maximum vertical displacement that cannot exceed the allowed value of  $[h_\sigma]$ ;  $\sigma_{\max}$  is the maximum tensile stress in canal lining and should be lower than the allowed  $[\sigma]$ .  $B_1$  is the width of joint opening;  $F$  is the total cost per unit length, with the subscripts of 1 to 3 represent the land expropriation, earth expropriation and canal

lining materials, respectively.  $A_c$  and  $A_q$  are the sectional areas of canal lining and filled gool without lining structure, respectively. This problem is thus simplified as a constrained optimization case with three geometric constrains and two performance constraints.

### 3.2 Computational procedure

Fig. 7 presents the specific procedure for computation and the detailed is as follows.

1) A cross section is assumed with geometric constraints satisfied, i.e.,  $m$ ,  $\alpha$  and  $d$  and both initial and boundary conditions input.

2) Thermal indexes are determined based on the initial thermal regime in the whole domain including  $C(T)$  and  $\lambda(T)$  and then one timestep of thermal computation is initiated with the duration of  $t_{\text{ther}} = N_{\text{ther}} * \Delta t_{\text{ther}}$ .

3) The frozen fringe is determined by a judgment statement of  $T_{ij} > T_f$  iterating through all cells. For elements at temperatures higher than the freezing point, the mechanical properties and hydraulic conductivity of thawed soils are specified while for those at temperatures within the range from  $-1^\circ\text{C}$  to the freezing point, the mechanical properties and hydraulic conductivity of 'warm' frozen soils are given. In this case, both the hydraulic and mechanical modes are turned on, i.e., *set ther off fluid on mech on*.

4) For elements with temperature higher than  $-1^\circ\text{C}$ , compression for this domain is calculated by a Drucker-Prager yield criterion with four characteristic mechanical parameters, i.e., elastic modulus, the Poisson's ratio, cohesion and angle of internal friction. Here, both the thermal and hydraulic computational modes are stopped and only the mechanical mode is activated, i.e., *set ther off fluid off mech on*.

5) Nodal and element information is recorded within one timestep and determine whether or not the computational duration exceeds the preset limit. If so, the computation is paused with the judgment of both the allowed deformation and tensile stress. Otherwise, computation for the next timestep initiates with thermal indexes determined based on the current degree of saturation and void ratio.

6) Determine whether the maximum vertical displacement is reached or not after the preset duration and the construction cost per unit length is subsequently calculated if a negative answer is gained. Otherwise, the geometric constraints of  $m$ ,  $\alpha$  and  $d$  are adjusted to be input in a new iteration.

7) Compare two successive construction costs calculated. If an allowed difference is reached, the geometric constraints corresponding to the optimized cost are determined.

## 4. Case study of an irrigation canal in loess plateau

### 4.1 Brief introduction to Jinghui Irrigation Area

The Jinghui Irrigation Area, located in the center of Shaanxi Province, is an artesian diversion work from Jing River. Terrains for this region inclined southeast, with slopes ranging from 1/300 to 1/600 and altitudes from 350

Table 3 Meteorological data for Jinghui irrigated area

Meteorological factor	Data
Annual mean precipitation / mm	538.9
Annual evaporation / mm	1212
Annual average sunshine hours / h	2200
Annual highest phreatic water level in winter / m	3.0
Annual daily average temperature lower than zero / $^\circ\text{C}$	50
Annual average freezing index / ( $^\circ\text{C}\cdot\text{d}$ )	77
Lowest daily average temperature / $^\circ\text{C}$	-13.6
Annual frozen depth / cm	20 - 40

Table 4 Physical parameters for foundation soils

Physical indexes	Data
Specific Gravity, $G_s$	2.69
Dry density, $\rho_d$ / $\text{g}/\text{cm}^3$	1.50
Atterberg limit	
Liquid limit, $w_L$ / %	33.9
Plastic limit, $w_p$ / %	18.7
Particle grading characteristics	
0.075 - 2.0 mm	10.4%
0.005 - 0.075 mm	65.3%
< 0.005 mm	24.3%

to 450 m. This irrigation area has been built and opened since the 1930s, with the total irrigated area of about  $9.69 \times 10^4$  hectares after extension, including gravity irrigated area of more than 76.4%. Five main canals with the total length of 80.6 km are set in this area, with twenty branches longer than 299.8 km. A branch canal lying at the second terrace of Jing River, the northern part of the irrigated area, is selected as a study object. The climate here can be classified as the continental semi-arid monsoonal climate. From meteorological stations in Jinghui Irrigation Area, the characteristic meteorological data for this region is summarized and presented in Table 3. The physical parameters for the foundation soils are listed in Table 4. The designed discharge is  $4.5 \text{ m}^3/\text{s}$  for this canal with the lining structure produced by C20 cast-in-place concrete. The roughness and longitudinal slope for the lining structure are 0.015 and 1/1500, respectively. This canal is not put into service in winter and the normal canal freeboard is 0.6 m.

### 4.2 Geometric model in computation and definite conditions

The slope orientation may result in considerable imbalance of heat absorption in both sides in that the selected canal runs from west to east. Here, the shady half of the section is taken in numerical modeling for sake of safety and the geometric model with sizes identical to the in-situ is employed here, as presented in Fig. 8. The highest underground water table based on several years' observation lies about 3.0 m, and a conservative value of  $h_1$ , equal to 10.0 m is taken to be the depth considered in computation while the depth labelled as  $h_2$  is 8.2 m taking into account

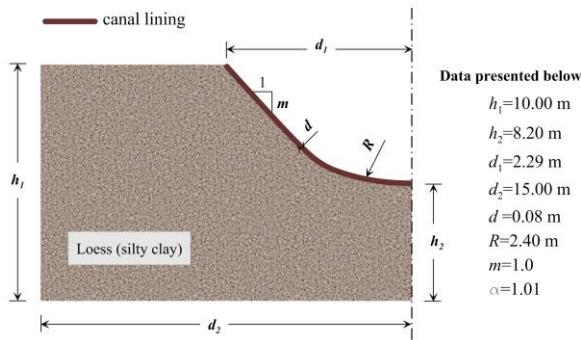


Fig. 8 Geometric model for numerical computation

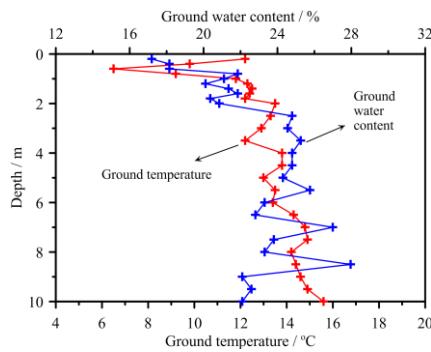


Fig. 9 In situ measured ground water content and temperature

both depth of flow and normal canal freeboard. The three geometric constraints of  $m$ ,  $\alpha$  and  $d$  for the practical cross section are 1.0, 1.01 and 0.08, respectively. Both sides of the geometric model in Fig. 8 are assumed as adiabatic and fixed nodal temperatures are applied and also the x-scale nodal displacement is fixed. A simplified constant thermal boundary is specified at the bottom of the model, with the y-scale nodal displacement fixed while at top boundaries, the daily average temperature in freezing period is given as the nodal temperature boundary, with free y-scale displacements for nodes. A seismic fault zone investigation carried out from 1998 to 2000 indicates that ground temperature at the depth of 10.0 m varies within a narrow range from 16.3 to 16.7°C (Li *et al.* 2001), proving little correlation with atmospheric circulation and thus an average temperature of 16.5°C is applied. While for the upper boundary, the annual average freezing index, a relatively stable meteorological data, is evenly distributed within the freezing period because the live monitored atmospheric temperature has shown great fluctuations. Thus, a lowest daily average temperature of -13.6°C is utilized here as the upper boundary for sake of safety. The in-situ measured profiles of ground temperature and water content are taken as the initial conditions for computation, as presented in Fig. 9.

#### 4.3 Determination of model parameters

Materials used in canal lining and joint sealing are assumed to be elastic. The mechanical parameters for concrete, joint sealing material and foundation loess are listed in Table 5. Note that the mechanical parameters for

Table 5 Mechanical properties of materials in canal

Type of materials	Parameters	Data
Concrete	$E$ , GPa	24
	$\nu$	0.167
	$\rho$ , kg/m <sup>3</sup>	2500
	$E$ , MPa	0.20
Joint sealing materials	$\nu$	0.45
	$\rho$ , kg/m <sup>3</sup>	1900
	$a_1$ , MPa	0.57
	$b_1$ , MPa/°C	0.55
Foundation soil	$a_2$	0.40
	$b_2$	-0.008
	$a_3$ , MPa	0.15
	$b_3$ , MPa/°C	0.055
	$a_4$ , °	12
	$b_4$ , °/°C	1.60

Table 6 Characteristic indexes for heat and water migration for loess

Indexes	Data
Specific heat, $C$ , kJ/(kg·°C)	
in frozen state	1.67
in thawed state	1.38
Heat conductivity, $\lambda$ , W/(m·°C)	
in frozen state	0.94
in thawed state	1.00
Permeability, $K(T_{ref})$ , 10 <sup>-7</sup> m/s	6.12
Unfrozen water content, $\theta_u$ , %	
$a$ , %/°C	17.67
$b$	0.70

concrete and joint sealing material are taken from the Technical code for seepage control engineering on canal (GB/T50600—2010, 2011) while those for the foundation soil obtained from the literature (Lai, *et al.* 2009). Here, the loess used as the foundation of irrigation canal is assumed to be elasto-plastic and its response to the overburden pressure can be described by the Drucker-Prager criterion.

The characteristic parameters for the migration of heat and water in loess are listed in Table 6. Here, the hydraulic conductivity for loess was measured at a reference temperature of 20°C while for soils at various minus-temperatures it can be adjusted based on the varying viscosity with respect to temperature (Wang, *et al.* 2016b).

#### 4.4 Results and analysis

Both the normal displacement and tensile stress in canal lining structure are calculated for the practical hydraulic section in Jinghui Irrigation Area based on the above frost heave theory. Results presented in Fig. 10 indicate that the maximum normal displacement occurs at the center of the arc-bottom, with the magnitude of  $d_{nor}$  equal to 1.82 cm,

Table 7 Comparison of practical and optimized hydraulic section

Type of section	Flow depth /m	Thickness of canal lining, $d$ /m	Slope, $m$	Radius of arc-bottom, $R$ /m	Opening width, $d_1$ /m	$\alpha$
Practical	1.200	0.080	1.0	2.400	5.59	1.01
Optimized	1.320	0.077	1.1	1.350	5.36	1.00

Table 8 Comparison of practical and optimized results

Type of section	Maximum normal displacement/cm	Maximum tensile stress/Pa	Concrete dosage/m <sup>3</sup>	Excavation/m <sup>3</sup>	Cost/RMB
Practical	1.82	$2.69 \times 10^6$	0.55	6.90	881.6
Optimized	2.45	$1.08 \times 10^6$	0.53	6.75	858.9

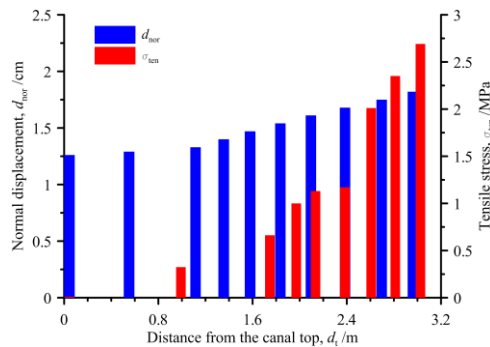


Fig. 10 Normal displacement and tensile stress in canal lining

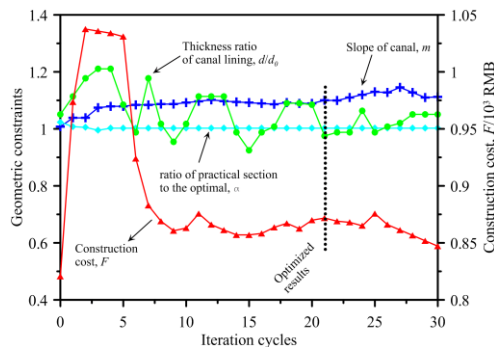


Fig. 11 Optimization procedure for considered variables

lower than the allowed deformation given by the design code of the Ministry of Water Resources of the PRC, i.e.,  $[h_{\sigma}] = 3.0$  cm. This can be classified as the recoverable deformation during spring thawing. Moreover, the failure of concrete materials is assumed to obey the first strength theory, i.e., the maximum tensile stress theory. This implies that the material will be fractured as the maximum tensile stress is reached, i.e.,  $\sigma = [\sigma]$ . Here for the case mentioned above, the maximum tensile stress calculated is  $2.69 \times 10^6$  Pa and exceeds the allowed stress level of  $[\sigma] = 1.10 \times 10^6$  Pa. Thus, the tensile failure may occur at the extremely harmful cases for the area considered and a more reliable size of hydraulic section should be optimized for sake of safety.

The structural computation initiates based on the above parameterized model and a file for optimized design is created with the target function of  $|F_j - F_{j-1}| \leq \delta$ , i.e., the iteration of computation terminated until the difference of

two successive calculated costs of construction lower than an allowed value of  $\delta$ . Here, a conservative value of  $\delta$  equal to 2 is specified. The cycles of iteration are controlled not less than 30 and the specific optimized procedure for computation is illustrated in Fig. 11, including the geometric constraints and construction cost. The optimal solution is obtained after 21 cycles of iteration. Comparison of characteristic sizes for both optimized and practical hydraulic sections is shown in Table 7. The flow depth for the considered section increases by 0.12 m while for canal lining, the thickness reduces by 0.3 cm and the slope of lining structure shows a slight increase. More importantly, the radius of arc-bottom for the optimized section decreases by 1.05 m, with the central angle lowers by  $5.4^\circ$ , implying a larger curvature for the arc-bottom. In this case, the arc effect is enhanced with the growing overall stiffness of lining structure, indicating that a more rational cross section will be obtained; however, the maximum normal displacement grows by 0.63 cm but is still lower than the allowed value of 3.0 cm, and the residual deformation during spring thawing can also be neglected. Besides, the maximum tensile stress decreases by 59.8%, lower than the allowed limit and it can be inferred that the optimized lining structure fully utilizes the strength of materials and the maximum value is restrained within the boundary. From Table 8, the opening width for the optimized section decreases by 0.23 m and for a unit length of 1.0 km, an area of 230 m<sup>2</sup> will be saved for the farm land. Also, the thickness of canal lining reduces by 0.3 cm and construction cost will be lowered by 2.6%, which is quite a considerable saving of investment for the whole irrigated area.

## 5. Conclusions

This paper carried out a novel numerical analysis on optimizing the cross section of irrigation canals in seasonal frozen ground and the main conclusions are as follows.

- A practical model for clayey soils was established by assuming that the frost heave originates from the phase transition of the migrated and in-situ water into ice, and its rationality was verified by a model test.

- The mathematical function for optimizing the hydraulic section of irrigation canals was proposed considering the hydraulic characteristics and failure modes induced by frost heave. Three characteristic sizes were taken as the geometric constraints while both the maximum normal displacement and maximum tensile stress as the constraints of mechanical performance, with the construction cost as the target function.

- A novel numerical approach was suggested for the hydraulic section optimization and solved three key technical problems, i.e., live computation of frost heave and compression in corresponding domains, synchronization of hydraulic and thermal calculations, and numerical implementation of the mathematical function of the hydraulic section.

- A typical cross section along the Jinghui Irrigation Canals was taken as the study object and the most harmful case with hydrogeological and meteorological data was considered in computation. Comparison of optimized and

practical sections proves that the maximum normal displacement is still lower than the allowed value and thus a more reliable canal running will be satisfied.

## Acknowledgements

This research was financially supported by the National Natural Science Foundation of China (No. 51778528, 51478385, 51574219 and 41572268) and the Importation and Development of High-Caliber Talents Project of Beijing Municipal Institutions granted to Dr. Jilin Qi (CIT&TCD20150101). These supports are greatly appreciated. In addition, the authors thank Professor Wei Wu at University of Natural Resources and Life Sciences, Vienna, Austria, for his strong support.

## References

- Akagawa, S. (1988), "Experimental study of frozen fringe characteristics", *Cold Reg. Sci. Technol.*, **15**(3), 209-223.
- Anderson D.M. and Tice A.R. (1973), *The Unfrozen Interfacial Phase in Frozen Soil Water System*, in *Physical Aspects of Soil Water and Salts in Ecosystems, Ecological Studies (Analysis and Synthesis)*, Springer, Berlin, Heidelberg, Germany.
- Arenson, L.U., Xia, D.D., Segó, D. and Biggar, K.W. (2005), "Brine and unfrozen water migration during the freezing of Devon silt", *Proceedings of the 4th Biennial Workshop on Assessment and Remediation of Contaminated Sites in Arctic and Cold Climates (ARCSACC)*, Edmonton, Alberta, Canada, May.
- Azmach, T.F., Segó, D.C., Arenson, L.U. and Biggar, K.W. (2012), "New ice lens initiation condition for frost heave in fine-grained soils", *Cold Reg. Sci. Technol.*, **82**, 8-13.
- Black, P.B. and Miller, R.D. (1990), "Hydraulic conductivity and unfrozen water content of air-free frozen silt", *Water Resour. Res.*, **26**(2), 323-329.
- Black, P.B. (1995), "Rigidice model of secondary frost heave", CRREL Report 95-12.
- Dash, J.G. (1989), "Thermomolecular pressure in surface melting: motivation for frost heave", *Science*, **246**(4937), 1591.
- GB/T50600-2010. (2011), *Technical Code for Seepage Control Engineering on Canal*, Appendix C, The ministry of Water Resources of the People's Republic of China, China Planning Press, Beijing, China.
- Huang, Q. (2014), "Impact evaluation of the irrigation management reform in northern China", *Water Resour. Res.*, **50**(5), 4323-4340.
- Itasca (1999), *FLAC Manual: Theoretical Background*, Itasca Consulting Group, Minneapolis, Minnesota, U.S.A.
- Konrad, J.M. (1993), "Sixteenth Canadian Geotechnical Colloquium: frost heave in soils: Concepts and engineering", *Can. Geotech. J.*, **31**(2), 223-245.
- Kujala, K. (1994), "Factors affecting frost susceptibility and heaving pressure in soils", Ph.D. Thesis, University of Oulu, Oulu, Finland.
- Lai, Y.M., Zhang, M.Y. and Li, S.Y. (2009), *Engineering Theory and Application in Cold Regions Engineering*, Science Press, Beijing, China (in Chinese).
- Lai, Y.M., Zhang, X.F., Xiao, J.Z., Zhang, S.J. and Liu, Z.Q. (2005), "Nonlinear analyses for frost-heaving force of land bridges on Qinghai-Tibet Railway in cold regions", *J. Therm. Stress.*, **28**(3), 317-331.
- Li, S.H., Wang, Y. and Cao, H.X. (2001), "Anomalous features of geotemperature in the depth of 10 m by Gaoling observation point before the 1998 Jingyang Ms4.8 earthquake, Shaanxi Province", *Northwest. Seismol. J.*, **23**(2), 117-119 (in Chinese).
- Li, S.Y., Zhang, M.G., Tian, Y.B., Pei, W.S. and Zhong, H. (2015), "Experimental and numerical investigation on frost damage mechanism of a canal in cold regions", *Cold Reg. Sci. Technol.*, **116**, 1-11.
- Liu, B. and Li, D.Y. (2012), "A simple test method to measure unfrozen water content in clay-water system", *Cold Reg. Sci. Technol.*, **78**, 97-106.
- Ma, W., Zhang, L. and Yang, C. (2015), "Discussion of the applicability of the generalized Clausius-Clapeyron equation and the frozen fringe process", *Earth-Sci. Rev.*, **142**, 47-59.
- Mei, Y., Hu, C.M., Yuan, Y.L., Wang, X.Y. and Zhao, N. (2016), "Experimental study on deformation and strength property of compacted loess", *Geomech. Eng.*, **11**(1), 161-175.
- Nixon, J.F. (1991), "Discrete ice lens theory for frost heave in soils", *Can. Geotech. J.*, **28**(6), 843-859.
- Qi, J.L., Sheng, Y., Zhang, J.M. and Wen, Z. (2007), "Settlement of embankments in permafrost regions in the Qinghai-Tibet Plateau", *Norw. J. Geogr.*, **61**(2), 49-55.
- Qi, J.L. and Zhang, J.M. (2008), "Definition of warm permafrost based on mechanical properties of frozen soils", *Proceedings of the 9th International Conference on Permafrost*, Fairbanks, Alaska, U.S.A., July.
- Qian, Z.Z., Lu, X.L., Yang, W.Z. and Cui, Q. (2014), "Behaviour of micropiles in collapsible loess under tension or compression load", *Geomech. Eng.*, **7**(5), 477-493.
- Qian, Z.Z., Lu, X.L., Yang, W.Z. and Cui, Q. (2016), "Comparative field tests on uplift behavior of straight-sided and belled shafts in loess under an arid environment", *Geomech. Eng.*, **11**(1), 141-160.
- Romanovsky, V.E. and Osterkamp, T.E. (2015), "Effects of unfrozen water on heat and mass transport processes in the active layer and permafrost", *Permafrost Periglac.*, **11**(3), 219-239.
- Thomas, H.R., Cleall, P.J., Li, Y., Harris, C. and Kern-Luetsch, M. (2009), "Modelling of cryogenic processes in permafrost and seasonally frozen soils", *Geotechnique*, **59**(3), 173-184.
- Wang, S.H., Qi, J.L., Yin, Z.Y., Zhang, J.M. and Ma, W. (2014), "A simple rheological element based creep model for frozen soils", *Cold Reg. Sci. Technol.*, **106**, 47-54.
- Wang, C.D., Zhou, S.H., Wang, B.L., Guo, P.J. and Su, H. (2016a), "Settlement behavior and controlling effectiveness of two types of rigid pile structure embankments in high-speed railways", *Geomech. Eng.*, **11**(6), 847-865.
- Wang, S.H., Qi, J.L., Yu, F. and Liu, F. (2016b), "A novel modeling of settlement of foundations in permafrost regions", *Geomech. Eng.*, **10**(2), 225-245.
- Watanabe, K., Mizoguchi, M., Ishizaki, T. and Fukuda, M. (1997), "Experimental study on microstructure near freezing front during soil freezing", *Proceedings of the International Symposium on Ground Freezing and Frost Action in Soils*, Lulea, Sweden, April.
- Yao, X.L., Qi, J.L. and Wu, W. (2012), "Three dimensional analysis of large strain thaw consolidation in permafrost", *Acta Geotech.*, **7**(3), 193-202.
- Yao, X., Qi, J., Liu, M. and Yu, F. (2016), "Pore water pressure distribution and dissipation during thaw consolidation", *Transport Porous Med.*, **116**(2), 1-17.
- Zakir, H.M., Islam, M.M. and Hossain, M.S. (2016), "Impact of urbanization and industrialization on irrigation water quality of a canal-a case study of Tongi canal, Bangladesh", *Adv. Environ. Res.*, **5**(2), 109-123.
- Zhu, Q. (1991), "Frost heave prevention measures for canal lining in China", *Irrig. Drain. Syst.*, **5**(4), 293-306.